ISSN 1330-3651
UDC/UDK 624.044:624.012.4.074.43

BUCKLING ANALYSIS OF CONCRETE SPHERICAL SHELLS

Ivana Mekjavić

Subject review

This paper presents a buckling analysis for several notable concrete thin shells around the world. An approach which takes into account the large deflection and plasticity effects was performed using Sofistik software to estimate the buckling load. A geometrically non-linear analysis of these structures with and without geometrical imperfections was performed. To take into account the possible plastification of the material a materially non-linear analysis was performed simultaneously with the geometrically non-linear analysis. The buckling analysis of concrete spherical shells shows that including only one kind of non-linearity does not give a realistic situation and only their combination results in the decreasing of ultimate failure load.

Keywords: *buckling analysis, concrete shells, spherical shells, geometrically non-linear analysis, materially non-linear analysis*

Analiza izbočavanja betonskih sfernih ljusaka

Pregledni članak

U ovom radu je prikazana analiza izbočavanja nekoliko značajnih betonskih sfernih ljusaka u svijetu. Pristup kojim se uzimaju u obzir velike deformacije i učinci plastičnosti primijenjen je uporabom programa Sofistik radi procjene opterećenja izbočavanja. Provela se geometrijski nelinearna analiza ovih konstrukcija sa i bez geometrijske imperfekcije. Da bi se uzela u obzir mogućnost plastifikacije materijala također se provela materijalno nelinearna analiza istodobno s geometrijski nelinearnom analizom. Analiza izbočavanja betonskih sfernih ljusaka pokazala je da se uključujući samo jedan tip nelinearnosti ne dobiva realno stanje te da samo njihovo kombiniranje dovodi do smanjenja graničnog opterećenja sloma.

Ključne riječi: *analiza izbočavanja, betonske ljuske, sferne ljuske, geometrijski nelinearna analiza, materijalno nelinearna analiza*

1 Introduction

In some simple two-dimensional structures it is sufficient to determine only the lowest value of the load at which buckling commences. However, in the case of shells, it may be also necessary to investigate the postbuckling behavior because it has an important bearing on the magnitude of the failure load.

The importance of the postbuckling behavior, which the small deflection theory of buckling is not capable of predicting, was discovered as a consequence of attempts to correlate experimental results with analytical predictions.

Poor correlation between the results of theory and experiment exists when both principal membrane forces are compressive, as in the case of cylindrical shells under axial compressive load; cylindrical shells under distributed load normal to the surface, which causes bending; and domes under inward radial pressure. If both the principal membrane forces are compressive, they tend to increase with deformation of the shell. After the initial buckling, the shell can only transmit loads smaller than the initial buckling load. This is particularly true for concrete shells because of creep and deviation of the actual shape of the shell from the assumed theoretical surface.

Good correlation exists when one of the principal membrane forces is tensile. If one of these forces is tensile, it tends to return the shell back to its original position, thus enabling it to carry loads greater than the initial buckling load.

In general, the value of the buckling load depends on shell geometry, type of restraint at boundary, material properties of shell, the location of reinforcing steel, and the type of load.

2 Buckling of domes

The classical analysis for the bifurcation buckling of spherical domes under axisymmetrical radial pressure q_{cr} was long ago found to be [1, 2]

$$q_{cr} = \frac{2Eh^2}{r^2\sqrt{3(1-\nu^2)}} \tag{1}$$

where:
E – modulus of elasticity, MPa
h – thickness of the shell, m
r – radius of the sphere, m
ν – Poisson's ratio.

The corresponding critical stress is therefore

$$\sigma_{cr} = \frac{q_{cr}\,r}{2h} = \frac{Eh}{r\sqrt{3(1-\nu^2)}}. \tag{2}$$

When the uniform external pressure q exceeds q_{cr}, given by equation (1), i.e., $q > q_{cr}$, the system is unstable. If $q = q_{cr}$ the spherical shell is in neutral equilibrium for small displacements. If $q < q_{cr}$ the shell is in stable equilibrium.

The value of critical stress defined by equation (2), which is based upon the small-displacement theory, often does not agree with experimental data. However, the real value of the critical stress is much lower than this. Experimental results have repeatedly shown critical stresses of as low as 10 percent of the classical, i.e., of that predicted by the small deflection theory [3]. By the use of large deflection theory of buckling and plasticity effects, results may be obtained which closely approximate experimental values. A spherical shell under radial external

pressure will buckle suddenly or "oilcan" by leaping to a lower state of energy at a stress far below that given by the classic value.

For practical applications we can use the following empirical formula for calculating q_{cr} [1]:

$$q_{cr} = \left(1 - 0{,}175\frac{\alpha° - 20°}{20°}\right)\left(1 - \frac{0{,}07r/h}{400}\right)(0{,}3E)\left(\frac{h}{r}\right)^2 \qquad (3)$$

which gives satisfactory results for $400 \le r/h \le 2000$ and $20° \le \alpha \le 60°$, where α is the angle between the axis of rotation and the dome edge.

Here an approach which takes into account the large deflection and plasticity effects was performed by using Sofistik software [4]. This approach is based on minimization of the energy of the system, i.e., energy methods. It also permits computation of the lower as well as the upper boundary of the buckling load, and is applicable to all types of shells.

3
Analyzed concrete spherical shells

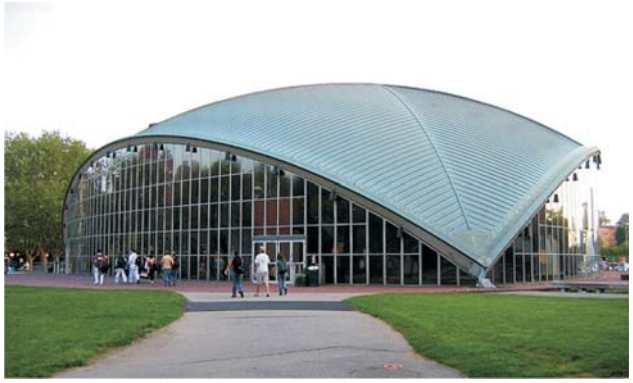

Figure 1 Kresge-MIT Auditorium, Boston, USA (Saariner, 1954)

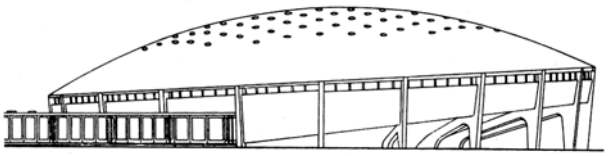

Figure 2 Ehime Public Hall, Matsuyama, Japan (Tange&Tsuboi)

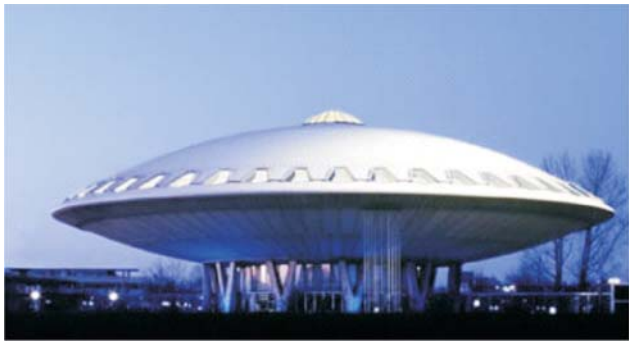

Figure 3 Het Evoluon, Eindhoven, Netherlands (Kalff, 1966)

Using the Sofistik finite element program that solves large-scale structural analysis problems, several spherical shell structures were examined.

Figs. 1-3 show some of the remarkable early shells for the Kresge – MIT auditorium in Boston, Ehime Public Hall in Matsuyama and Het Evoluon in Eindhoven.

These structures were built before the use of computers. Prior to the availability of computers and the finite element method, shells were analyzed using approximate methods which forced the designer to develop an intuitive feel for the structural behaviour of the shell, which is sometimes missing with the uncritical use of computers.

Structural analysis and the optimization study of these shells were also performed using Sofistik software in [5].

3.1
Kresge Auditorium

The Kresge Auditorium at MIT, designed by a noted modernist architect, Eero Saarinen, consists of a one-eighth spherical segment dome-shaped concrete roof enclosing a triangular area approximately 49 m (160 ft) on a side. The dome is entirely supported on three points at the vertices of the triangle. The total weight of the roof is approximately 1500 tons, and the thickness of the roof shell is 8,9 cm (3,5 in) which is increased near the edge beams up to 14 cm. The 8,9 cm (3,5 in) concrete shell is covered with 5,1 cm (2 in) of glass fiberboard and a second non-structural layer of lightweight concrete 5,1 cm (2 in) thick. Additions had to be made to this structure, since Saarinen's sculptural cutting of the shell created severe edge disturbances to the membrane stresses in the shell that had to be counteracted by an edge beam (45,7 cm (18 in) height). There were also large stresses created at the three points of support. These were reinforced with tapered H-shaped steel ribs, which in turn were connected to a steel hinge allowing for movement. In the end, after the formwork was removed it was discovered that the edges were deflecting an unacceptable amount (clearly well over 12,7 cm (5 in)) due to uncontrolled creep. Additional supports were added in the form of (4-by-9-in) steel tubes spaced at 3,35 m (11 ft), which are also used to support the window wall [6].

The problems with this building did not end with the solution of the structural problems. The shell was difficult and unusual to construct, and significant difficulties were encountered in concrete placement (poor consolidation), protection of the reinforcing steel (inadequate concrete cover) and above all in the waterproofing the roof of the building. The satisfactory solution of these problems had to wait until decades after the commissioning of the building and through several trials of different roofing procedures.

The original neoprene roofing was later replaced with lead-coated copper roofing and then copper roofing. The repair of the construction was costly and forced the closure of the building for a few months.

3.2
Ehime Public Hall

The Ehime Public Hall in Matsuyama, Japan, designed by Japanese engineers, Tange and Tsuboi, is a shallow spherical inclined shell supported by 20 columns. A ring is provided around the base between columns. The thickness of the shell is 8 cm with a diameter of 49,35 m and a rise of 7 m at the crown [7].

3.3
Het Evoluon

The Het Evoluon in Eindhoven was the last major project of the Netherlands designer Louis Kalff. The building is unique due to its resemblance to a landed flying

saucer, which makes it look very futuristic. The dome has a diameter of 77 m and rests on 12 V-shaped columns. The overall height of the building is 30 m [7].

4
Buckling analysis of concrete spherical shells using finite element analysis

The existence of large-scale computer programs makes it possible to study non-linear behavior in such shells. An analysis according to the third-order theory which contains non-linear analysis plus analysis according to the second-order theory and additionally the effects of the geometrical system modification, e.g. snap through, length modification for big deformations, and behavior after buckling was performed. Non-linear effects (e.g. plasticising, cracks) can be analyzed only with iterations. This is done in Sofistik's module ASE with a modified Newton method with constant stiffness matrix. The advantages of the method are that the stiffness matrix does not have to be decomposed more than once and that the system matrix remains always positive definite. The Linesearch method with the update of the tangential stiffness matrix is utilized for problems according to the second-order theory. The load increment is reduced here internally according to the available residual forces. If an iteration step proceeds into the right direction, i.e. in the direction of an energy minimum, then a new tangential stiffness which enhances the further iteration's behavior is generated, if necessary. Cracked elements are considered here also with a reduced stiffness.

By means of the concrete law one can even consider creep and shrinkage effects for a cracked shell-element (the redistribution of stress, from concrete to the reinforced steel, due to creep and shrinkage).

The numerical studies on these structures illustrate one of three basic problems that need to be considered in design beyond the stress analysis: (1) initial geometrical imperfections, (2) concrete cracking and steel yielding, and (3) large deflections.

The concrete material properties assume a unit weight of 25 kN/m^3, the Young's Modulus of 36 GPa (C45/55) and the Poisson's ratio of 0,2. The reinforcing steel material properties assume the yield strength of 500 MPa and the Young's Modulus of 200 GPa. The load on the structure is its self weight and snow load of 1,25 kN/m^2 uniformly distributed on the horizontal projection.

In Sofistik FEA program, the Sofiplus was used as pre-processing tool for model building and mesh generation. The plane quadrilateral or triangular shell element (in the case of MIT Auditorium) was used in meshing.

4.1
Geometrically non-linear analysis

An ultimate load iteration in geometrical non-linear analysis of these structures with and without imperfections in geometry was performed. As construction tolerances cannot be overly refined without making field costs prohibitive, some imperfections are always present in shells and the problem mainly is to set limits and recognize how such imperfections influence behavior and thereby control the resulting response by adequate reinforcement.

A regular ultimate load iteration in geometrical non-linear analysis without geometrical imperfection is started at first with constant snow load for the Ehime dome. It ends with a load factor of 48,30. Displacements of the last stable load case with load factor 48,30 are shown in Fig. 4.

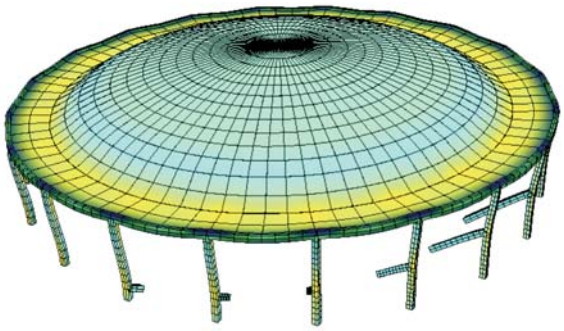

Figure 4 Displacements of last stable load case with load factor of 48,30 in the Ehime dome without geometrical imperfection

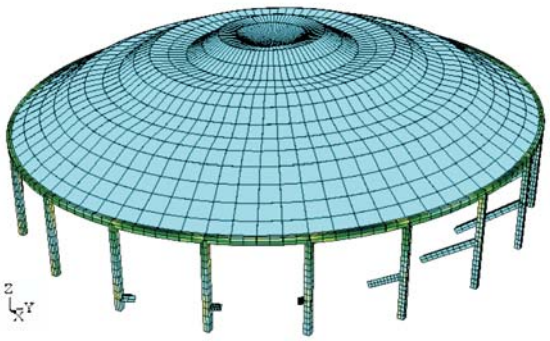

Figure 5 First buckling shape on undeformed structure for Ehime dome

Using the stress state of the snow load case the buckling mode shapes are determined considering the element stresses on undeformed system. The first buckling mode shape is applied scaled as non-stressed imperfection (Fig. 5). The imperfection has here a maximum value in global X direction of 20 mm.

An ultimate load iteration geometrically non-linear follows with consideration of this imperfection. It ends now already with the load factor 19,10. Last load step displacements with load factor 19,10 are shown in Fig. 6.

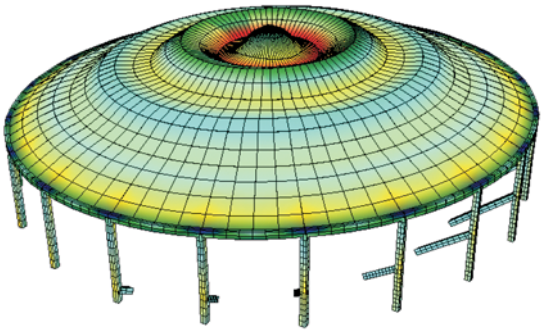

Figure 6 Displacements of last stable load case with load factor of 19,10 in the Ehime dome with geometrical imperfection

In the case of geometrical non-linear analysis the stiffness is calculated for the deformed structure. Since the last stable load case during an ultimate load iteration is always considered as primary load case, the program generates always the new tangential geometric stiffness matrix.

A buckling eigenvalue determination as well as a concurrent eigenvalue analysis are available in Sofistik's module ASE. Buckling eigenvalues on deformed structure can be determined with the last stable load case of ultimate load iteration as primary load case. Here, the buckling

eigenvalue determination gives a buckling factor of 1,08 for the first buckling mode on deformed structure with geometrical imperfection, as shown in Fig. 7. For comparison, the buckling factor of 99,12 is obtained for the first buckling mode on undeformed structure with the snow load as primary load case i.e. under the stresses of the primary load case (Fig. 5). The geometric stiffness from the primary load case for buckling eigenvalues is scaled with the buckling factor.

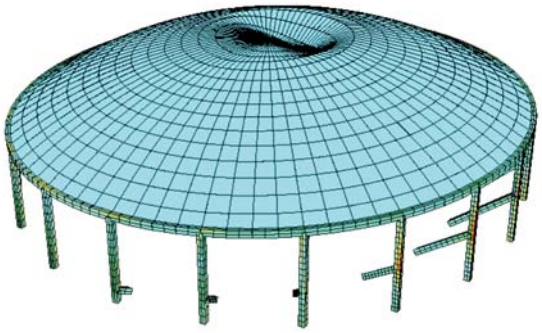

Figure 7 First buckling shape on deformed structure with geometrical imperfection for Ehime dome

The critical buckling load for a spherical shell under radial pressure according to the theory of elasticity, i.e., classical equation of buckling (1) amounts to q_{cr} = 121,16 kN/m^2. The value for the snow load uniformly distributed on the horizontal projection is obtained from $q'_{cr} = q_{cr}/\cos^2\alpha$ = 167,10 kN/m^2 with $\alpha = 31{,}62°$. To relate theoretical values to actual test data the critical buckling load according to empirical relation (3) amounts to q_{cr} = 24,85 kN/m^2. The value for the snow load uniformly distributed on the horizontal projection is obtained from $q'_{cr} = q_{cr}/\cos^2\alpha = 34{,}27$ kN/m^2, where $\alpha = 31{,}62°$.

The program calculates a value for the critical buckling load of 60,38 kN/m^2 (48,30·1,25) according to the third-order theory without geometrical imperfection. An analysis according to the third-order theory with geometrical imperfection gives a critical buckling load value of 23,88 kN/m^2 (19,10·1,25).

The value of critical load 167,10 kN/m^2 defined by classical equation, which is based upon the small-displacement theory does not agree with ultimate load results of 60,38 kN/m^2 and 23,88 kN/m^2. This discrepancy is explained by applying the large-deflection theory of buckling, which takes into account the squares of the derivatives of the deflection, initial geometrical imperfections and a host of additional factors. The ultimate load result of 23,88 kN/m^2 is in satisfactory agreement with the empirical solution of 34,27 kN/m^2.

A plot of a limit load iteration for the node number with the largest displacement can be generated. Load-deformation curves with and without geometrical imperfections are drawn for the node with the maximum vertical displacement, as shown in Fig. 8. With the first ultimate load iteration (curve A) a ramification problem without geometrical imperfection is processed. The deformations increase almost linearly; from a specific point (ramification point) no further load increase is more possible. Curve B shows the load deformation curve with the geometrical imperfection from the first scaled buckling mode shape. The ultimate load is smaller now, what on one hand results from the scheduled deformation (u-0) and on the other hand, however, the load deformation curve of a shell has in general a reducing curve after the ramification point, that one can imagine from the point A to the point B. The reducing curve cannot be processed currently with the module ASE.

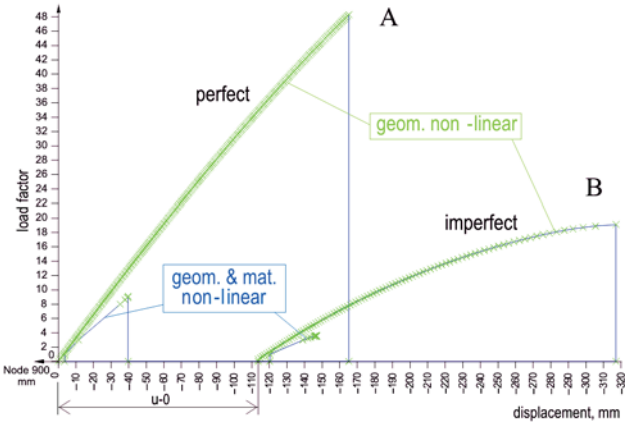

Figure 8 Load-deformation curves with and without geometrical imperfections for the node with the largest vertical displacement in Ehime dome

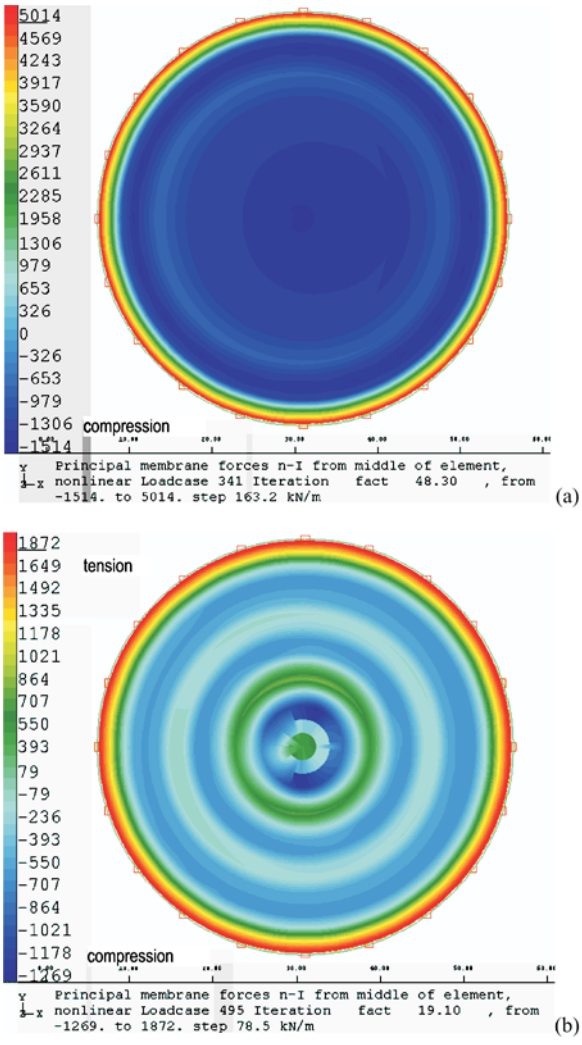

Figure 9 Principal membrane forces in the Ehime dome (a) without and (b) with geometrical imperfection

The effects of the shell rise on the value of the critical buckling load are analyzed for the Ehime shell with and without geometrical imperfection. The values for diameter

Table 1 Effect of rise *d* on principal membrane forces and buckling load for Ehime dome

Rise *d* /m	Loading	System without imperfection			System with imperfection		
		Buckling load factor	Principal membrane forces / kN/m		Buckling load factor	Principal membrane forces / kN/m	
			Min. compressive	Max. tensile		Min. compressive	Max. tensile
7	Dead load	–	–54,4	170,0	–	–126,8	162,2
	Snow load	48,30	–2500,0	5014,0	19,10	–2353,0	1872,0
8	Dead load	–	–53,6	147,3	–	–100,1	145,0
	Snow load	64,00	–2820,0	5576,0	25,50	–2330,0	2221,0
9	Dead load	–	–53,8	130,6	–	–59,6	127,1
	Snow load	80,30	–2944,0	5983,0	37,10	–1917,0	2776,0

(span) and thickness of Ehime shell are kept constant. The dimensions of the ring and columns are equal to 40×60 cm and 50×50 cm, respectively. The slope of the shell is set equal to 2°. The only variable that is changed is rise *d*. The rise *d* varies from 7, 8 and 9 meters in this study.

Tab. 1 gives the effects of rise *d* on the principal membrane forces and the buckling load for a spherical shell with a uniform thickness of 8 cm. It is seen that if the principal radii of curvature of the shell surface are larger (that is, the shell is flatter), the membrane forces are generally greater. Hence the value of the buckling load will be lower, possibly substantially lower. Increasing the rise by cca 30 % increases the buckling load factor by a factor of about 2.

Typically, applying initial geometrical imperfection related to the first buckling mode, the buckling load for the system without imperfection is reduced by a factor of about 2,5.

In addition, it is seen that the compressive hoop forces of the Ehime dome under snow load change to tension when geometrical imperfection in the form of the first buckling mode shape with a maximum deviation of 20 mm occurs. Fig. 9 shows the principal membrane forces for the Ehime dome with and without geometrical imperfection. Since this initial geometrical imperfection leads to tension in hoop direction it is mandatory to include this possibility in the layout of the steel reinforcement of the shell.

It should be noted that such observation is not verified on the Ehime dome with rise $d = 9$ m.

Notice also that the buckling of the Ehime shell results in excessive principal tensile membrane forces which are restricted to a narrow zone at the edge of the dome. These tensile forces produce too high stresses in the reinforced concrete and should be reduced by increasing the edge ring size (stiffness).

4.2 Interaction of the non-linearities

The analyzed concrete spherical shells are also used to demonstrate the interaction of the two main non-linearities, material and geometrical.

An analysis with non-linear (elasto-plastic) material was performed simultaneously with a geometrically non-linear analysis.

The material behavior of reinforced concrete can be described by the following properties: non-linear stress-strain curve in tensile and compressive zone, contribution of the concrete between cracks (tension stiffening), non-linear material behavior of the steel reinforcement and simplified check of the shell's shear stress.

The buckling load obtained by a static geometrically non-linear analysis and a combination of geometrically and materially non-linear analysis of spherical shells is given in Tab. 2.

For the Ehime shell the stable ultimate load calculations geometrically and materially non-linear end now at about 11,30 kN/m^2 (9,04·1,25) and 4,48 kN/m^2 (3,58·1,25) for the system without and with geometrical imperfections respectively. Hence, the buckling load in the materially non-linear, large deformation analysis is reduced by a factor of 5,3. Applying initial geometrical imperfection in the form of the first buckling mode shape with a maximum deviation in global X direction of 20 mm, the buckling load for the system without imperfection is reduced by a factor of about 2,5. An iso-area presentation of the plastified zones leads to Fig. 10.

The maximum bottom non-linear von Mises stresses are equal to 12,70 and 7,26 MPa for the system without and with geometrical imperfections, respectively. Fig. 11 shows the resulting von Mises stress state with high stress concentrations in the vicinity of the concentrated supports. A slight geometrical deviation (related to the first buckling

Table2 Buckling load obtained by a geometrically non-linear and a combination of geometrically and materially non-linear analysis of spherical shells

Name of construction	System without imperfection			System with imperfection		
	Buckling load factor		Non-linear von Mises tensile stress / MPa	Buckling load factor		Non-linear von Mises tensile stress / MPa
	Geometrically non-linear	Geometrically and materially non-linear		Geometrically non-linear	Geometrically and materially non-linear	
Kresge A. - design 1	2,70	0,78	5,83	3,90	0,78	5,83
Kresge A. - design 2	8,00	0,72	5,06	8,20	0,72	5,06
Kresge A. - design 3	14,80	1,29	4,79	15,20	1,29	4,79
Het Evoluon	67,70	1,05	3,04	46,10	1,05	3,04
Ehime Public Hall	48,30	9,04	12,70	19,10	3,58	7,26

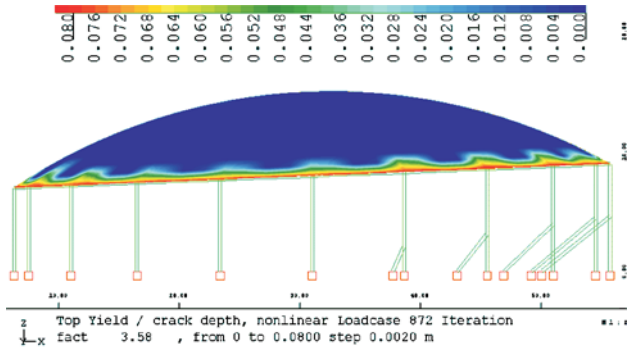

Figure 10 Plastified zones in the Ehime dome with geometrical imperfection resulting from geometrical and material nonlinear analysis

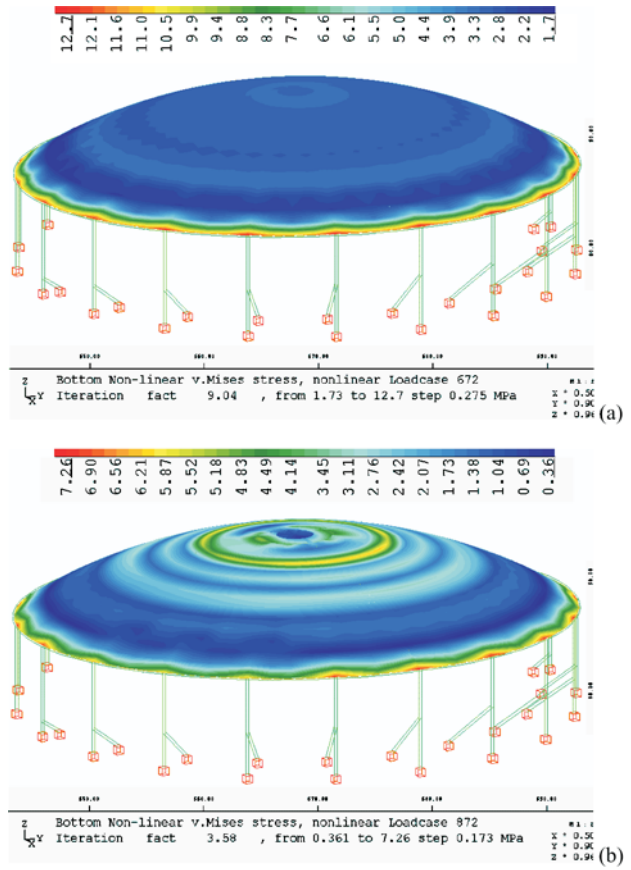

Figure 11 Bottom non-linear von Mises stresses in the Ehime dome (a) without and (b) with geometrical imperfection

mode) may lead to greater stresses towards the apex of the dome as shown in Fig. 11 (b) compared to (besides the edge bending effect) a homogeneous stress state shown in Fig. 11 (a).

In [5] it had been shown that structural optimization of Kresge Auditorium results in a distribution of larger thickness around the supports equal to 30 cm.

Here the critical buckling load and the von Mises stresses on the shell surface for three different designs are compared (Tab. 2).

In the original design 1 the concrete shell with a uniform thickness of 8,9 cm is strengthened with a stiffening beam (20×45 cm) around the perimeter of the building, and the concrete class is C30/37 [8]. In the design 2 the concrete strength of the distributed thickness shell and 20×45 cm edge beam is C40/50. The design 3 comprises distributed thickness shell and (30×30 cm to 30×70 cm) edge beam with higher concrete strength C45/55.

The maximum bottom non-linear von Mises stresses are equal to 5,83 MPa, 5,06 MPa and 4,79 MPa for the design 1, design 2 and design 3, respectively (Tab. 2). These maximum von Mises stresses occur in the region of the supports, gradually decreasing to approximately zero at the center of the shell (Fig. 12). It has also been found that the design 3 develops less tensile area and smaller maximum tensile stresses obtained by a linear analysis, and thus is a more efficient design. Also, the deflections for the distributed thickness shells (design 2 and 3) were much smaller than the uniform thickness shell (design 1). In addition, it can be shown that the edge beam of uniformly varying cross section (height varies from 30 cm at apex to 70 cm at supports) in design 3 enhances the shell stiffness, reducing maximum (principal) tensile stresses and deflection, and thereby reducing reinforcements. Also, the higher concrete strength of C45/55 reduces the deflection and the amount of reinforcements.

Here the critical buckling load obtained by a geometrically non-linear analysis is maximized for the Kresge shell by structural optimization. Optimization is based on the structure without geometrical imperfection leading to a buckling load factor of 14,80 (Tab. 2). Also the maximum geometrical deviation in global X direction of 20 mm was introduced in an additional simulation assuming an imperfection shape taken from the first buckling mode. In this example, the initial geometrical imperfection (corresponding to the first buckling shape) increases the final load level to 15,20 because it enhances the curvature of the shell roof. Including the two main non-linearities, material and geometrical, the buckling load is reduced to 1,29 showing the strong influence of the non-linear material

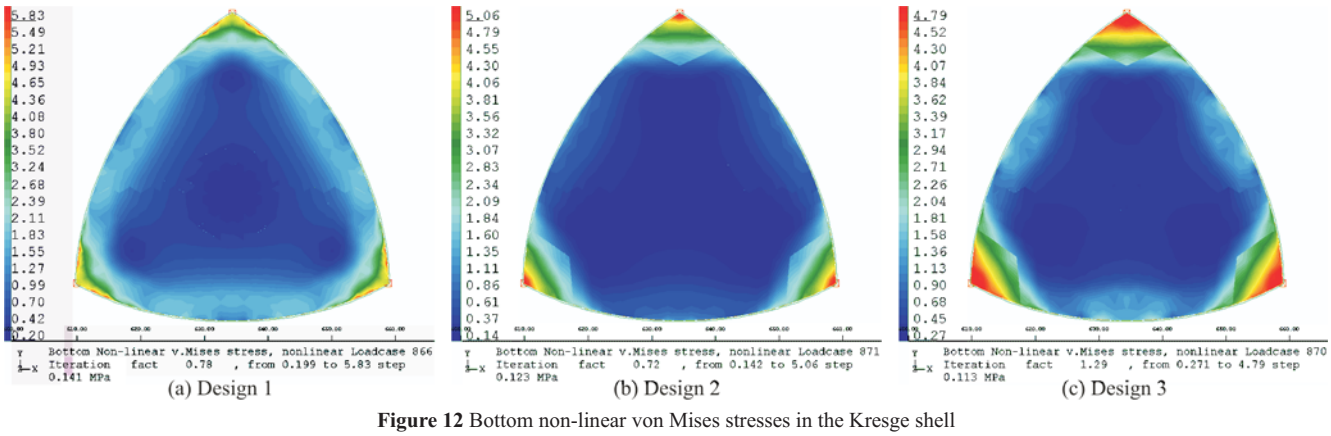

Figure 12 Bottom non-linear von Mises stresses in the Kresge shell

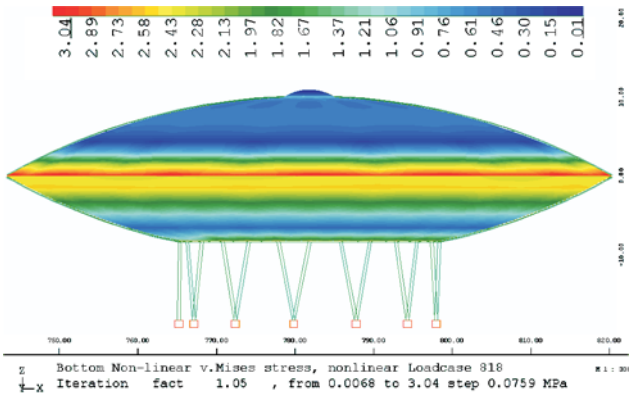

Figure 13 Bottom non-linear von Mises stresses in the ribbed Evoluon shell

behavior on the structural response.

This important interaction is also demonstrated by the Evoluon shell. As can be found in [5] structural optimization of Evoluon results in a shell with uniform thickness of 8 cm, reinforced with meridional and hoop ribs. The ribbed model built in Sofistik has a 20×30 cm ring at the top of the dome around 6,70 m diameter skylight. Radiating off of the ring beam at the top of the dome are 30×60 cm ribs at 7°. Added are two hoop 30×60 cm ribs that are located at 6 m, and 12,2 m from the edge ring. The edge ring at the junction of the upper and lower shell is 40×60 cm with a 77 m diameter. A 60×80 cm bottom ring is supported by 80×80 cm V-shaped columns. The lower shell also has two hoop 30×60 cm ribs that are located at 6 m, and 15,4 m from the edge ring.

In this example, the buckling load factor of 67,70 obtained by a geometrically non-linear analysis for the structure without geometrical imperfection is reduced to 46,10 by the initial geometrical imperfection related to the first buckling shape (with the maximum deviation of 20 mm in global X direction) showing a substantial sensitivity (Tab. 2). Tab. 2 also shows that the buckling load obtained by a combination of geometrically and materially non-linear analysis is significantly reduced to 1,05. The maximum bottom non-linear von Mises stress is equal to 3,04 MPa. Fig. 13 shows the von Mises stresses on the shell surface for Evoluon.

From Tab. 2 the following conclusions can be drawn: including only one kind of non-linearity does not give a realistic situation and their combination results in the decreasing ultimate failure load.

5 Conclusion

From a detailed structural buckling assessment of analyzed concrete spherical shells it can be concluded that shells can be extremely sensitive with respect to slight deviation of their ideal parameters like initial geometry, boundary conditions etc. Initial geometrical imperfections and non-linearities tend to prevent the most real structures from achieving their unrealistically high failure loads. To get a more accurate answer nonlinear analysis should be carried out, taking into account geometrical imperfections, material non-linearities, edge effects which cause bending etc., provided the shell is less prone to a sudden buckling failure.

In the finite element buckling analysis of concrete spherical shells, consideration shall be given to the possible substantial reduction in the value of the buckling load caused by large deflections, material non-linear effects, and the deviation between the actual and theoretical shell surface.

6 References

[1] Timoshenko, S. P.; Gere, J. M. Theory of Elastic Stability. Second Edition. International Student Edition. McGraw-Hill, Singapore, 1963.
[2] Billington, D. P. Thin Shell Concrete Structures. Second Edition. McGraw-Hill, New York - Toronto, 1982.
[3] Bradshaw, R. Application of the General Theory of Shells. // Journal of the American Concrete Institute. 58, 2(1961), 129-148.
[4] Sofistik Software Version 2010
[5] Mekjavić, I.; Pičulin, S. Structural Analysis and Optimization of Concrete Spherical and Groined Shells. // Tehnički vjesnik. 4, 17(2010), 537-544.
[6] Ford, E. R. The Details of Modern Architecture. Volume 2: 1928 to 1988. The MIT Press, Cambridge, Massachusetts, 2003.
[7] Rile, H. Prostorne krovne konstrukcije. Građevinska knjiga, Beograd, 1977.
[8] http:/www.arche.psu.edu/thinshells/module III/case_study_3.htm

Author's addresses:

Doc. dr. sc. Ivana Mekjavić, dipl. ing. građ.
University of Zagreb
Faculty of Civil Engineering
Kačićeva 26
10000 Zagreb, Croatia
e-mail: ivanam@grad.hr